Scientific Researches in
Theoretical and Applied Physics
Vol. 2, Issue. 2, Fall 2024

Research Paper

# Investigation of envelope solitary space charge waves and modulational instability in intense charged particle beams

**Abdolrsoul Esfandyari Kalejahi*[1]**



DOI: 10.22034/strap.2024.17977

**Refference to this article:** Esfandyari Kalejahi, A (2024). Investigation of envelope solitary space charge waves and modulational instability in intense charged particle beams. *Scientific Researches in Theoretical and Applied Physics*, 2 (2): 1-18

**Keywords**

**Received: 2023/12/09**
**Accepted: 2024/05/14**
**Available: 2025/07/08**

**A B S T R A C T**

The space charge waves in a long coasting charged particle beam is investigated in the context of water-bag distribution for the longitudinal distribution function. The nonlinear propagation of modulated space charge wave packets is studied, by employing a fluid beam model. It is revealed that dispersion curve obtained in linear approximation consists of two forward ($0 \leq k < \sqrt{2}/2$) and backward ($\sqrt{2}/2 < k \leq 1$) segments so as they are connected at a frequency cutoff point where the group velocity becomes zero. $k$ denotes normalized wavenumber. Considering small yet weakly nonlinear deviations from equilibrium, and using multiple-scale method, the basic set of fluid equations is reduced to a nonlinear Schrödinger equation (NLSE) for the slowly varying linear charge perturbation amplitude. It is remarked that the dispersion coefficient in NLSE doesn't depend on σ, and it is negative in $0 < k < 1$ range which means negative group velocity dispersion. $\sigma$ denotes a dimensionless parameter which depends on the beam equilibrium pressure and linear charge density, electric charge of beam particle and geometric parameter$g_0$ Finally, the analysis reveals that both of stable dark and instable bright excitations associated with space charge waves can propagate not only in normal dispersion (forward waves) region but also in anomalous dispersion (backward waves) region.

* **Corresponding Author: Abdolrsoul Esfandyari Kalejahi**
**E-mail:** esfand@tabrizu.ac.ir

1. Faculty of Physics, University of Tabriz, Tabriz, Iran

مقاله پژوهشی

# بررسی امواج بار فضایی سالیتونی پوش دار و ناپایداری مدولاسیونی در باریکه های ذره باردار شدید

عبدالرسول اسفندیاری کلجاهی[1]*



ارجاع به این مقاله: اسفندیاری کلجاهی ، عبدالرسول (1403). بررسی امواج بار فضایی سالیتونی پوش دار و ناپایداری مدولاسیونی در باریکه های ذره باردار شدید. *پژوهش‌های علمی در فیزیک نظری و کاربردی*، 2(2): 1-18.

DOI: 10.22034/strap.2024.17977

چکیده

The space charge waves in a long coasting charged particle beam is investigated in the context of water-bag distribution for the longitudinal distribution function. The nonlinear propagation of modulated space charge wave packets is studied, by employing a fluid beam model. It is revealed that dispersion curve obtained in linear approximation consists of two forward ($0 \leq k < \sqrt{2}/2$) and backward ($\sqrt{2}/2 < k \leq 1$) segments so as they are connected at a frequency cutoff point where the group velocity becomes zero. $k$ denotes normalized wavenumber. Considering small yet weakly nonlinear deviations from equilibrium, and using multiple-scale method, the basic set of fluid equations is reduced to a nonlinear Schrödinger equation (NLSE) for the slowly varying linear charge perturbation amplitude. It is remarked that the dispersion coefficient in NLSE doesn't depend on σ, and it is negative in $0 < k < 1$ range which means negative group velocity dispersion. $\sigma$ denotes a dimensionless parameter which depends on the beam equilibrium pressure and linear charge density, electric charge of beam particle and geometric parameter $g_0$ Finally, the analysis reveals that both of stable dark and instable bright excitations associated with space charge waves can propagate not only in normal dispersion (forward waves) region but also in anomalous dispersion (backward waves) region.

کلیدواژه‌ها

دریافت شده: 1402-09-18

پذیرفته شده: 1403-02-25

منتشر شده: 1404-04-17

* نویسنده مسئول: عبدالرسول اسفندیاری کلجاهی

رایانامه: esfand@tabrizu.ac.ir

- استاد، دانشکده فیزیک، دانشگاه تبریز، تبریز

## I. INTRODUCTION

The longitudinal space-charge waves and instabilities in high current accelerators play an important role in the dynamics of intense beams for accelerator applications [1,2]. Historically, the study of space-charge waves goes back to Simon Ramo and W.C. Hahn in vacuum tubes [3,4]. In the 1950s, Birdsall and Whinnery performed calculations of gain and phase of electrons passing near lossy walls which was used for beam amplification [5]. It is, therefore, very important to fully understand such phenomena in order to develop advanced accelerators for various applications. For example, beam dynamics including the space-charge waves and instabilities can be found in induction accelerators as drivers for heavy ion inertial fusion [6].

Analytical solution of space-charge wave equation based on the cold fluid model in one dimension predicts two eigenmodes (the one is forward fast wave and the other is the backward slow wave), given an initial perturbation [7].

On the other hand, for most of machines of the transport of high intensity beams, especially near the source and injector, there is an internal repulsion due to space-charge forces. This process can introduce nonlinear forces that cause a reduction in beam quality. The longitudinal space charge waves can be generated by a perturbation to the beam density or energy in turn resulting from small errors in the applied fields. These kinds of perturbations give rise to instabilities that disrupt the beam under certain circumstances [8-13].

The experimental measurements concerning the propagation of space-charge waves with large amplitudes in an intense, charged-particle beam demonstrate that experimental observations begin to deviate from predictions of linear theory due to nonlinear effects [14]. Employing a large-amplitude perturbation by a UV laser, the evolution of the space charge wave under nonlinear effects has been observed [15]. The large-amplitude perturbations of solitary kind, a nonlinear structure which is a combination of sinusoidal wave trains, on an intense electron beam has experimentally been observed [ 16]. Theoretically, one of the most important equations describing such nonlinear phenomena is the Korteweg-deVries (KdV) equation [ [17-19]. These single pulse solitons are formed when nonlinear effect balances dispersion effect. Space-charge solitary waves in charged particle beams in resistive-wall transport channels has theoretically been studied by H. Suk et al [20]. They have shown that both slow and fast solitary waves can propagate so that the slow space-charge solitary waves grow in amplitude, while the fast space-charge solitary waves decay. Assuming a water-bag distribution for the longitudinal distribution function, it has been revealed that

weakly nonlinear perturbations moving near the sound speed evolve according to KdV equation [21]. The existence of solitary waves traveling along a coasting ion beam in circular accelerators has been investigated by Schamel and Fedele based on a new coupled system of equations, the Vlasov equation and a generalized form of Poisson's equation [22]. Two-dimensional particle-in-cell simulations have represented that the electrostatic solitary waves can excite and propagate in ion beam neutralization by injecting electrons from a filament [23].

On the other hand, there exist localized wave structures (known as envelope solitons) which are deduced when the nonlinearity in the system is balanced by the wave group dispersion. The dynamics of such structures are governed by Nonlinear Schrödinger equation (NLSE) [24]. Noticing the observations of envelope soliton structures in the laboratory and space plasma [25, 26], the modulational instability (MI) has received a great attention during last several decades (see e. g, [27-34].

As far as the space charge waves are concerned, Stephan I. Tzenov and Ronald C. Davidson [35] obtained a nonlinear Schrödinger equation for the slowly varying single-wave amplitude using the renormalization group (RG) technique [36-39], in an intense particle beam propagating through a smooth focusing field.

In nonlinear optics, NLSE describes the formation and evolution of the so-called dark and bright solitons. The dark solitons are called holes or cavitons in the case of charged particle beam.

Another important aspect of NLSE is that it provides a description of collective behavior of charged-particle beams. In fact, though, the conventional description of collective behavior of charged-particle beams is usually given in terms of the Vlasov equation, however, some alternative descriptions have been extended in terms of NLSE governing the collective dynamics of the beam while interacting with the surrounding medium [40-42]. A self-consistent model for the longitudinal dynamics of a long, coasting beam in linear geometry in the smooth-focusing approximation has been investigated and consequently a closed system of equations for the nonlinear evolution of the longitudinal distribution function has been found [43]. Besides, it has been shown that in the case of a beam with uniform phase-space density, the Vlasov–Maxwell equations can be replaced exactly by the hydrodynamic equations with a triple adiabatic pressure lawcoupled with the Maxwell equations [44].

Based on Ref. 43, it has previously been demonstrated that in the case of constant phase-space density (assuming a water-bag distribution for the longitudinal distribution function) the Vlasov–Poisson equations are fully equivalent to a

hydrodynamic model with zero heat flow and triple-adiabatic equation-of-state [21].

The layout of manuscript is as follows. In section II, we repeat the hydrodynamic equations derived as a key for the subsequent analysis for illustration. In section III, we obtain NLSE using the standard reductive perturbation technique (multiple scales). The purpose of section IV is to review modulational stability and instability analysis of NLSE based on linearizing around the monochromatic wave solution, and the solutions of NLSE. Section V devotes to numerical analysis. Finally, conclusions are drawn in section VI.

## II. THE MODEL EQUATIONS

The present paper devotes to the theoretical investigation of self-modulation in intense charged particle beams. We consider longitudinal disturbances in a long coasting beam with characteristic radius $r_b$ in which beam particles have charge $e_b$ and rest mass $m_b$. It is supposed that the beam propagates in the direction $z$ in a linear geometry. In addition, it is assumed that the beam propagates through a straight, perfectly conducting cylindrical pipe with wall radius $r_w$. We also assume axial kinetic energy of the beam in z direction is $E_{k,b} = (\gamma_b - 1)m_b c^2$, where $\gamma_b = (1-\beta_b)^{-1/2}$denotes the relativistic mass factor and $c$ is the speed of light *in vacuo*. The average axial velocity of the beam particles is given with $V_b = \beta_b c$. Besides, we assume the applied transverse focusing force is modeled in the smooth focusing approximation. Finally, the thin-beam (paraxial) approximation is employed to treat the nonlinear dynamics of the beam particles, and the particle motions in the beam frame are assumed to be nonrelativistic. Assuming a water-bag distribution for the longitudinal distribution function, the fluid dynamical (moment) equations for charged particle beam [21] include the normalized density (continuity) equation

$$\frac{\partial \eta}{\partial T} + \frac{\partial (U\eta)}{\partial Z} + \frac{\partial U}{\partial Z} = 0, \tag{1}$$

and the normalized momentum equation

$$\frac{\partial U}{\partial T} + \frac{\partial \eta}{\partial Z} + \frac{U\partial U}{\partial Z} + \sigma\eta\frac{\partial \eta}{\partial Z} + \frac{\partial^3}{\partial Z^3}\eta = 0, \tag{2}$$

Wher

$$\sigma = U_{bT}^2/(U_{b0}^2 + U_{bT}^2) = \frac{3P_{b0}}{e_b^2 g_0 \rho_{b0}^2 + 3P_{b0}}, \tag{3}$$

$$\eta = \frac{\lambda_b - \lambda_{b0}}{\lambda_{b0}}, \tag{4}$$

and

$$U = \frac{V_b}{\sqrt{U_{bT}^2 + U_{b0}^2}}. \tag{5}$$

In Eqs (1) and (2), the scaled (dimensionless) time variable $T$ and spatial variable $Z$ are defined by

$$T = \left(\frac{U_{bT}^2 + U_{b0}^2}{U_{b2}^2}\right)\frac{U_{b2}t}{r_w}, \tag{6}$$

$$Z = \sqrt{\frac{U_{bT}^2 + U_{b0}^2}{U_{b2}^2}}\frac{z}{r_w}. \tag{7}$$

where $U_{bT} = \sqrt{3P_{b0}/\lambda_{b0}m_b}$ denotes the thermal speed, $U_{b0} = \sqrt{3\lambda_{b0}\, g_0 e_b^2/m_b}$ denotes the effective sound speed associated with the geometric factor $g_0$, $U_{b2} = \sqrt{3\lambda_{b0}\, g_2 e_b^2/m_b}$ is an effective speed that measures the strength of the cubic dispersive term associated with the geometric factor $g_2$.

In the relation (4), the quantities $\lambda_b$ and $\lambda_{b0}$ represent the perturbed and unperturbed linear densities, respectively. Finally, the quantity $P_{b0}$ in the definition of $U_{bT} = \sqrt{3P_{b0}/\lambda_{b0}m_b}$ represents the unperturbed pressure.

## III. DERIVATION OF AN AMPLITUDE EVOLUTION EQUATION

In order to derive an explicit evolution equation describing the modulated envelope propagation, we shall use the standard reductive perturbation technique (multiple scales) [see Refs. 30-32]. To do this, we employ the stretched coordinates as $\xi = \varepsilon(Z - \lambda T)$ and $\tau = \varepsilon^2 T$ instead of independent variables $Z$ and $T$; here, $\lambda$ is a free (real) parameter, which is to be later related to the wave's group velocity by compatibility requirements and $\varepsilon$ is a small (real) parameter. The dependent variables $\eta$ and $U$ are expanded as

$$\eta = \sum_{n=1}^{\infty}\sum_{l=-\infty}^{+\infty} \varepsilon^n \eta_l^{(n)}(\xi,\tau)e^{il(kZ-\omega T)}, \qquad (8)$$

$$U = \sum_{n=1}^{\infty}\sum_{l=-\infty}^{+\infty} \varepsilon^n U_l^{(n)}(\xi,\tau)e^{il(kZ-\omega T)}, \qquad (9)$$

where the real parameters $\omega$ and $k$ are the wave's frequency and wavenumber respectively; the reality condition $A_l^{(n)^*} = A_{-l}^{(n)}$ is satisfied by all state variables; the star superscript denotes the complex conjugate of the (complex) harmonic amplitudes. Substituting the expansions (8) and (9) and the stretched variables $\xi$, $\tau$ into Eqs (1) and (2), the $n$th order reduced equations are obtained by choosing the coefficients of $\varepsilon^{n}$ equal to zero. We, therefore, obtain

$$-\lambda\frac{d}{d\xi}\eta_l^{n-1} + \frac{d}{d\tau}\eta_l^{n-2} - il\omega\eta_l^n + ilkU_l^n + \frac{d}{d\xi}U_l^{n-1} + \sum_{n'}\sum_{l'}[il'k\,\eta_{l'}^{n'}U_{l-l'}^{n-n'} + \frac{d}{d\xi}(\eta_{l'}^{n'}U_{l-l'}^{n-n'-1})] = 0, \qquad (10)$$

$$\frac{d}{d\tau}U_l^{n-2} - \lambda\frac{d}{d\xi}U_l^{n-1} - il\omega U_l^n + \mathrm{ilk}\eta_l^n + \frac{d}{d\xi}\eta_l^{n-1} + \sum_{n'}\sum_{l'}[il'kU_{l-l'}^{n-n'}U_{l'}^{n'} + U_{l-l'}^{n-n'-1}\frac{d}{d\xi}U_{l'}^{n'}] + \sigma\sum_{n'}\sum_{l'}[il'k\eta_{l-l'}^{n-n'}\eta_{l'}^{n'} + \eta_{l-l'}^{n-n'-1}\frac{d}{d\xi}\eta_{l'}^{n'}] + \frac{d^3}{d\xi^3}\eta_l^{n-3} + 3(\mathrm{ilk})\frac{d^2}{d\xi^2}\eta_l^{n-2} + 3(ilk)^2\frac{d}{d\xi}\eta_l^{n-1} + (ilk)^3\eta_l^n = 0. \qquad (11)$$

The first-order ($n=1$) equations yield

$$-l\omega\eta_l^{(1)} + lkU_l^{(1)} = 0\,, \qquad (12)$$

$$-l\omega U_l^{(1)} + l(k-k^3)\eta_l^{(1)} = 0\ . \qquad (13)$$

As a compatibility requirement for l=1, Eqs (12) and (13) give rise to the following dispersion relation

$$\omega^2 = k^2(1-k^2)\ . \qquad (14)$$

One must note that the dispersion relation (14) can also obtain from Eqs. (1) and (2) with linearization. Only real solution is thus obtained for the frequency ω, defined by

$$\omega = k\sqrt{1-k^2}, \qquad (15)$$

for $0 \le k \le 1$ .

We note that $\omega \to 0$ as $k \to 0$, i.e. for small *k*, the space charge wave has acoustic characteristics (mode). For small *k*, this acoustic mode behaves as $\omega \approx k$.

The group velocity $v_g$ is given by

$$v_g = \frac{\partial\omega}{\partial k} = \frac{1-2k^2}{\sqrt{1-k^2}}. \qquad (16)$$

The dispersion, the phase velocity and the group velocity curves obtained above are depicted in Figures 1a, 1b and 1c, respectively.

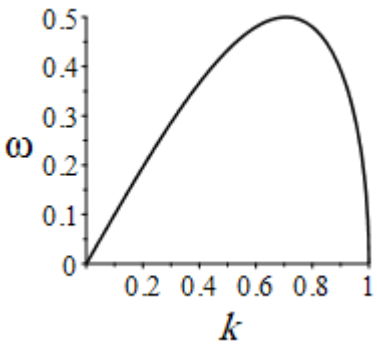


(a)

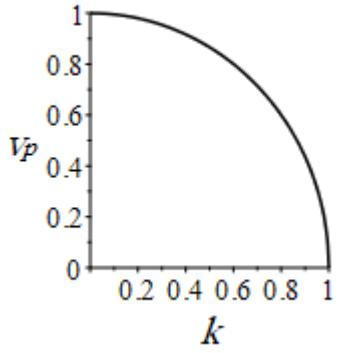


(b)

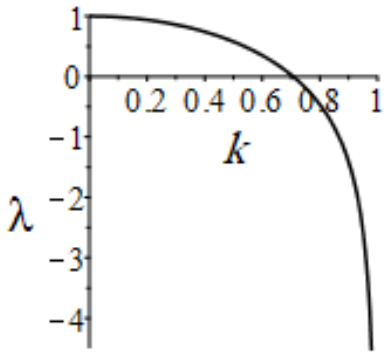


(c)

**Fig. 1** a) the dispersion curve, b) the phase velocity curve and c) the group velocity curve is depicted versus the wavenumber

For *n=1* and *l=1*, the relationship between $\eta_1^{(1)}$ and $U_1^{(1)}$ is determined as

$$U_1^{(1)} = \frac{\omega}{k}\eta_1^{(1)} \qquad (17)$$

For $n$ = 2 and $l$ = 1 (first harmonics), Eqs (10) and (11) lead to the following compatibility condition:

$$\lambda = \frac{1-2k^2}{\sqrt{1-k^2}} \qquad (18)$$

It is clear that the real parameter $\lambda$ equals to the group velocity $v_g = \partial\omega/\partial k$.

The group velocity behaves as $\lambda \approx 1 - 3/2k^2$ in very long-wavelength limit whereas it behaves as $\lambda \approx -\frac{1}{2}\sqrt{1/(1-k)}$ in short-wavelength limit $k \to 1$.

Although the linear dispersion relation (15) has very simple mathematical structure, however, it involves several interesting phenomena. If we take the maximum of the dispersion curve where $\omega = \omega_{max}$ for $k \equiv k_r = \sqrt{1/2}$ the group velocity will be zero. It is pointed out that the phase velocity neither becomes zero nor infinite at zero group velocity (ZGV) point. The wave propagation is, therefore, prohibited and only standing waves can exist. Zero group velocity (ZGV) takes place in a spatially periodic medium for electromagnetic waves [45]. Standing oscillations have been observed for electron cyclotron harmonic (ECH) waves [46] and also for electrostatic waves in a nonextensive electron-ion plasma [47]. Since the reflection and resonance phenomena occur when $k \to 0$ and $\to \infty$ respectively, the ZGV point is quite different from the resonance and reflection points.

Note that, $\omega_{max}$ denotes frequency cutoff for charge space wave. For $0 < k < k_r$, we have a forward acoustic branch because $\omega \to 0$ in the limit $k \to 0$ as stated above and both of the phase and group velocities have same directions i.e. $v_{ph} = \omega/k > 0$ and $\lambda > 0$. At the point $k=k_r$ where the dispersion curve turns downward is the branch-conversion state.

On the other hand, after the branch -conversion point $k_r$ the phase and group velocities become antiparallel since $v_{ph} = \omega/k > 0$ and $\lambda < 0$ in $k_r < k \leq k_{max} = 1$ range. This means that the segment of the dispersion curve with negative slope denotes the backward branch. For definition of forward and backward waves see Ref. 48.

The dispersion relation (15) reveals that the phase (group) velocity tends to zero ($-\infty$) as $k \to k_{max} = 1$. Note that, $2\pi/k_{max}$ denotes cutoff wavelength. It is noticeable that the group velocity corresponds to the actual signal velocity only when normal dispersion occurs, or, more generally, when the group velocity is less than the phase velocity. Some authors consider anomalous dispersion region where the dispersion curve has negative slope [49]. Sometimes, anomalous dispersion occurs when the group velocity is bigger than the phase one, so that it does not necessarily represent the actual propagation speed of any information or energy which is well-known phenomena in optics. In fact, in anomalous dispersion, the group velocity goes through both negative and positive infinite values [50,51]. Accepting this view point that the magnitude of group velocity should be less than

that of the phase one, we can say that our charged particle beam system represents anomalous dispersion for $\sqrt{-2+2\sqrt{5}}/2 < k \leq 1$ range because the absolute value of the group velocity is bigger than the phase one in this region; although the kind of wave is backward. In addition, the normal dispersion occurs in $0 \leq k < \sqrt{-2+2\sqrt{5}}/2$ range where the magnitude of the group velocity is less than the phase one. The group and phase velocities are both positive in $0 \leq k < \sqrt{2}/2$ range, i.e. forward region, while the phase (group) velocity is positive (negative) in $\sqrt{2}/2 < k < \sqrt{-2+2\sqrt{5}}/2$ range, i.e. backward region. At the point $k = \sqrt{-2+2\sqrt{5}}/2$, the magnitude of the group velocity equals to phase velocity.

Proceeding to $n = 2$, $l = 2$ in combination with $n = 3$, $l = 0, 1$ in equations (10) and (11), we obtain the nonlinear Schrödinger equation (NLSE):

$$i\frac{\partial\varphi}{\partial\tau} + P\frac{\partial^2\varphi}{\partial\xi^2} + Q|\varphi|^2\varphi = 0, \quad (19)$$

**which describes the slow evolution of the first-order amplitude of the beam density perturbation $\varphi \equiv \eta_1^{(1)}$.**

In summary, for a coasting beam described by water-bag distribution, it is proven that disturbances moving near the sound speed $\sqrt{U_{bT}^2 + U_{b0}^2}$ satisfy the nonlinear Schrödinger equation (Eq. 19).

The dispersion and nonlinear coefficients *P* and Q are given as

$$P = \frac{k(2k^2-3)}{2(1-k^2)^{\frac{3}{2}}} \quad (20)$$

$$Q = \frac{140k^8-(158\sigma+423)k^6+(18\sigma^2+305\sigma+458)k^4-(22\sigma^2+161\sigma+199)k^2+4\sigma^2+20\sigma+24}{k\sqrt{1-k^2}(144k^4-140k^2+24)}. \quad (21)$$

It is easy to prove that the dispersion coefficient *P* is related to the dispersion curve as $P = \partial^2\omega/2\partial k^2$. **It should be noticed that to investigate the existence of localized pulse solitons for every physical system, it is necessary to be obtained NLS Equation distinctly. In fact, the coefficients of dispersion term P and nonlinear term Q will be different for different physical systems. Hence, many numerous papers have been published due to obtaining NLSE for different nonlinear physical systems (for instance see Refs.27-34). For instance, in Ref. 34, the study of dust ion acoustic (DIA) modulation mode in a dusty plasma with superthermal electrons has been done. It is remarked that the dispersion and nonlinearity coefficients given in Refs. 27-34 are completely different with those in Eq. 19 although the form of nonlinear Schrodinger equation is the same.**

## IV. THE SOLUTIONS OF THE NONLINEAR SCHRÖDINGER EQUATION (ENVELOPE EXCITATIONS)

Exact expressions for envelope structures of the NLS equation (19) can be obtained by substituting $\varphi = \sqrt{\rho}e^{i\theta}$ into Eq. (19). The final formulae are found in Ref. [34] (also given e.g. in [32]), therefore, we here only briefly summarize the results. We obtain the *bright* envelope soliton

$$\rho = \rho_0 \,\mathrm{sech}(\tfrac{\xi - u\tau}{l})^2 \quad \theta = \tfrac{1}{2P}[u\,\xi - \left(\Omega + \tfrac{u^2}{2}\right)\tau], \tag{22}$$

in the case of $PQ>0$, and the *dark* envelope soliton

$$\rho = \rho_1[1 - \mathrm{sech}(\tfrac{\xi - u\tau}{\acute{l}})^2 \quad \theta = \tfrac{1}{2P}[u\,\xi - \left(\tfrac{u^2}{2} - 2PQ\rho_1\right)\tau], \tag{23}$$

for $PQ<0$. In Eqs. (22) and (23), the pulse widths $l$ and $\acute{l}$ are given by $l = \sqrt{2\,P/Q\rho_0}$ and $\acute{l} = \sqrt{2|P/Q\rho_1|}$, respectively. The *bright* envelope soliton represents a localized pulse, whereas, the *dark* one represents a localized region of negative wave density perturbation. Both of the *bright* and *dark* envelope solitons travel at a speed $u$. In addition of *dark* and *bright* envelope solitons, it is possible to find the *gray envelope soliton* as

$$\rho = \rho_2[1 - a^2\,\mathrm{sech}(\tfrac{\xi - u\tau}{l''})^2 \quad \theta = \tfrac{1}{2P}\Big[u\,\xi - \left(\tfrac{u^2}{2} - 2PQ\rho_2\right)\tau + \theta_{1,0}\Big] - s\,\sin^{-1}\frac{a\tanh\frac{\xi - u\tau}{l''}}{\sqrt{1 - a^2\,\mathrm{sech}(\frac{\xi - u\tau}{l''})^2}} \tag{24}$$

in which $\theta_{1,0}$ is a constant phase, $s = signP \times sign(u - V_0)$, $l'' = (1/a\sqrt{2|P/Q\rho_2|})$, $a^2 = 1 + (u - V_0)^2/(2PQ\rho_2) \le 1$ and $V_0$ is an independent real constant which satisfies the condition $V_0 - \sqrt{2|PQ|\rho_2} \le u \le V_0 + \sqrt{2|PQ|\rho_2}$. The *gray envelope soliton* represents a localized region of negative wave density with a finite amplitude at the origin in contrast to the black envelope soliton. One would notice that the *gray envelope soliton* transforms to *dark* one for $V_0 = u$, because $a=1$ in this case.

## V. MODULATIONAL STABILITY AND NUMERICAL ANALYSIS

The stability analysis of the NLSE (19) based on linearizing around the monochromatic wave solution $\varphi = \hat{\varphi}\,\exp(iQ\hat{\varphi})$ is easily obtained by choosing $\hat{\varphi} = \hat{\varphi}_0 + \epsilon\hat{\varphi}_1$ in which the perturbation $\hat{\varphi}_1 = \hat{\varphi}_{1,0}\exp(i(\hat{k}\xi - \hat{\omega}\tau))$. So, the dispersion relation is given by $\hat{\omega}^2 = P\hat{k}^2(P\hat{k}^2 - 2Q|\hat{\varphi}_0|^2)$. One must note that the perturbation wavenumber $\hat{k}$ and frequency $\hat{\omega}$ are different from the carrier wave quantities $k$ and ω. The wave will be stable if the product $PQ$ *is negative*. On the other hand, in the case of positive $PQ$, instability appears for perturbation wavenumber values below a critical value $\hat{k}_{cr} = \sqrt{2\,P/Q}\,|\hat{\varphi}_0|$. The maximum instability growth rate $\gamma_{max} = Q|\hat{\varphi}_0|^2$is achieved at $\hat{k} = \hat{k}_{cr}/\sqrt{2}$. Generally, the instability condition depends only on the sign of the product $PQ$.

It may be interesting to trace the asymptotic behavior of these coefficients for small *k*, i.e. for a large wavelength and around the singular points. *P* and *Q* behave as $P \approx -(3/2)k$ and $Q \approx (\frac{1}{6}\sigma^2 + \frac{5}{6}\sigma + 1)\frac{1}{k}$ for small *k*. On the other hand, *P* and *Q* behave as $P \approx -\frac{1}{8}\frac{\sqrt{2}}{(1-k)^{3/2}}$ and $Q \approx \frac{3\sigma}{28}\sqrt{\frac{2}{1-k}}$ for the wavenumbers very close to 1. Therefore, we conclude that *Q* tends to zero (∞) in the limit $k \to 1$ for $\sigma = 0$ ($\sigma \neq 1$). $P/Q$ is, therefore, negative (prescribing modulational stability, as we shall see) and behave as $PQ \approx -(\frac{1}{4}\sigma^2 + \frac{5}{4}\sigma + \frac{3}{2})$ for small *k* (i.e. in the long-wavelength limit) while $\frac{P}{Q} \approx -\frac{36}{4\sigma^2+20\sigma+24}k^2$ in the same limit. On the other hand, *P/Q* behaves as $\frac{P}{Q} \approx \frac{7}{6\sigma}\frac{1}{1-k}$ for $\sigma \neq 0$ and $\frac{P}{Q} \approx -\frac{7}{16}\frac{1}{(k-1)^2}$ for $\sigma = 0$ in the limit of *k=1*. So, the modulational stability (instability) occurs for $\sigma = 0$ ($\sigma \neq 0$) in the short-wavelength limit, $k \to 1$, as we shall see.

*Q* has also two excess singular points between 0 and 1 points, $k_{s1} = \sqrt{2}/3$ and $k_{s2} = \sqrt{3}/2$. *Q* behaves as $Q \approx \frac{47(7+9\sigma)\sqrt{2}}{13608}\frac{1}{(k-\frac{\sqrt{2}}{3})}$ and $Q \approx \frac{(-\frac{1}{32}+\frac{7}{96}\sigma-\frac{1}{24}\sigma^2)}{(k-\frac{\sqrt{3}}{2})}$ for $k_{s1} = \sqrt{2}/3$ and $k_{s2} = \sqrt{3}/2$, respectively. We note that *Q* becomes zero in the limit $k \to \sqrt{3}/2$ for both of $\sigma = 3/4$ and $\sigma = 1$.

Now, we return to numerical analysis and consider three values for the parameter $\sigma$ ($\sigma=0$, $\sigma=0.5$ and $\sigma=1$). We should note that $\sigma=0$ ($\sigma=1$) corresponds to very cold i.e. $e_b^2 g_0 \rho_{b0}^2 \gg 3P_{b0}$ (hot i.e. $e_b^2 g_0 \rho_{b0}^2 \ll 3P_{b0}$ ) charged particle beam according to the relation 3. In these two cases, the localized envelope structures do not depend on the characteristics of the beam, including the geometric parameters, particle charge, equilibrium density of the beam, etc. Furthermore, if $\sigma=0.5$, then the relation between the different equilibrium parameters of the beam will be satisfied as $P_{b0} = 1/3 e_b^2 g_0 \rho_{b0}^2$.

First, we notice that the dispersion coefficient, *P*, does not depend on the parameter $\sigma$ and it is ever negative in $0 \leq k \leq 1$ range. *P* tends to zero (-∞) in the limit of *k=0* (*k=1*). The plot of *P* versus *k* in $0 \leq k \leq 1$ range is depicted in figure 2. It is remarked that for very low wavenumbers, the dispersion coefficient *P* becomes very small so that the NLSE-based analysis fails because higher-order nonlinearity takes over which is a well-known phenomenon in nonlinear optics.

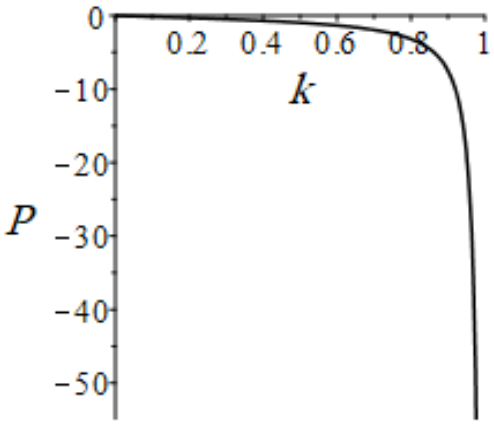

**Fig. 2** The dimensionless dispersion coefficient *P* in the NLS equation against the reduced normalized wavenumber.

Also, it will be interesting to find the wavenumbers for which the nonlinear coefficient *Q* tends to zero and infinity. In contrast with *P*, *Q* depends on the parameter $\sigma$. We saw the dispersion relation (20) represents forward linear oscillations for the segment $0 < k \leq \sqrt{2}/2$ and backward ones for the segment $\sqrt{2}/2 \leq k \leq 1$. Therefore, we consider stability analysis for two segments, separately. Focusing on the forward segment, it is remarked that *Q* will be zero at some points, says $k=k_{ZNP}$, for different values of $\sigma$. The subscript *ZNP* denotes zero nonlinearity point. The plot of $k_{ZNP}$ versus $\sigma$ has been depicted for the forward segment in figure 3. This figure shows that $k_{ZNP}$ at first decreases with the increase of $\sigma$ until it approaches minimum value then it increases as $\sigma$ increases. We note that $Q>0$ for $k< k_{ZNP}$ and $Q<0$ for $k> k_{ZNP}$.

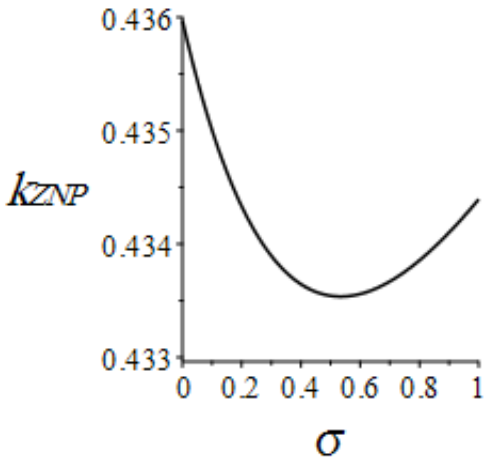


**Fig. 3** The plot of $k_{ZNP}$, in which the nonlinear coefficient in NLSE namely $Q=0$, versus dimensionless parameter σ for the forward segment of dispersion relation defined by Eq. 15.

On the other hand, there are some wavenumbers, says, $k=k_{INP}$, for which the nonlinear coefficient *Q* becomes singular. The subscript *INP* denotes infinity nonlinearity point. It is simply clear that $k_{INP}=0$ and $\sqrt{2}/3$ for every $\sigma$ as we saw above. Moreover, $Q \to +\infty$ as $k \to k_{INP}=0$ and $Q \to -\infty\,(+\infty)$ as $k \to k_{INP}=\sqrt{2}/3$ from left (right) side. We have remarked that the sign of the coefficient product *PQ* determines the stability profile and the type of space charge localized envelope excitations ($PQ < 0$ for stable dark type envelope solitons and $PQ > 0$ for instable bright type envelope ones). Therefore, we deduce that the stable dark (instable bright) excitations can propagate in $0 < k < k_{ZNP}$ $(k_{ZNP} < k < \sqrt{2}/3)$ range. For the wavenumbers higher than $k_{INP} = \sqrt{2}/3$ up to $k=\sqrt{2}/2$ only the stable dark excitations can propagate. Figure 4 shows the variation of *Q* versus the wavenumber in range $0 < k < \sqrt{2}/2$ which confirms above points.

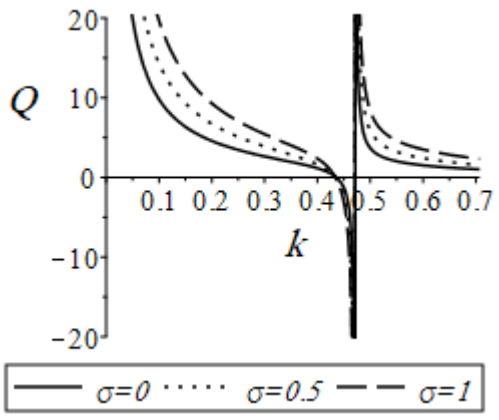


**Fig. 4** The dimensionless nonlinear coefficient *Q* in the NLSE against the reduced normalized wavenumber for the forward segment of dispersion relation defined by Eq. 15.

Now, we concentrate on the backward segment $\sqrt{2}/2 < k \leq 1$. Figures 5 illustrates the points in $\sigma$-$k$ plane on which the numerator (solid curve) and denominator (dashed line) of $Q$ tends to zero. Fig. 5b represents the zoomed curves in range $0.6 < \sigma < 1$. The solid curve in figure 5 shows that $k_{ZNP}$ at first decreases with the increase of $\sigma$ until it approaches minimum value then it increases as $\sigma$ increases.

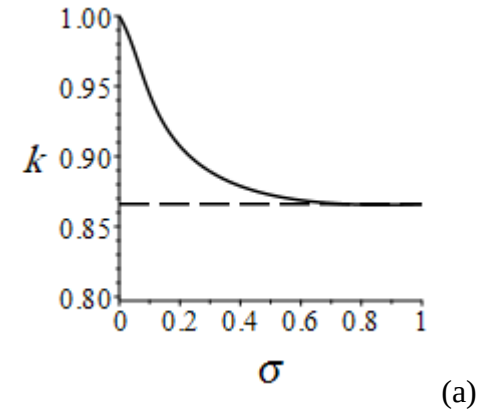


(a)

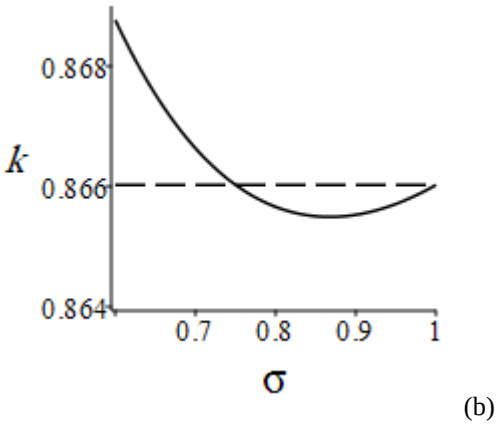


(b)

**Fig. 5.** a) the plots of the points in $\sigma$-$k$ plane on which the numerator (solid curve) and denominator (dashed line) of the dimensionless nonlinear coefficient $Q$, for the backward segment of dispersion relation defined by Eq. 15, tends to zero in $0 < \sigma < 1$ range, b) same plots as zoomed in range $0.6 < \sigma < 1$.

It is evidence from Fig. 5b that two curves intersect at two points $(3/4, \sqrt{3}/2)$, and $(1, \sqrt{3}/2)$ where $Q \approx 3.849$. So, we conclude that the wavenumber $k$=$\sqrt{3}/2$ is not singular point of $Q$ for $\sigma = 3/4$ and $\sigma = 1$ so as only the stable dark type envelope solitons can propagate. Besides, it is remarked that $k_{ZNP} > k_{INP}$ for $\sigma < 3/4$ meanwhile $k_{ZNP} < k_{INP}$ for $\sigma > 3/4$ where $k_{INP} = \sqrt{3}/2$ . Also, it is observed that Q is singular at the point $k_{INP} = \sqrt{3}/2$ provided $\sigma \neq 3/4$ as remarked above. We find $Q>0$ in the range $\sqrt{2}/2 \leq k < k_{INP} = \sqrt{3}/2$ for $\sigma < 3/4$ , namely the stable dark type envelope solitons can propagate. Q will be negative for the wavenumbers higher than $k_{INP} = \sqrt{3}/2$ up to $k_{ZNP}$, hence the instable bright ones will propagate. In addition, we obtain $Q>0$ for the wavenumbers higher than $k_{ZNP}$ up to *1* so that the stable dark type envelope solitons appear, again. Figure 6 shows the variations of $Q$ versus the wavenumber in range $\sqrt{2}/2 \leq k \leq 1$ for $\sigma < 3/4$ which confirms above points.

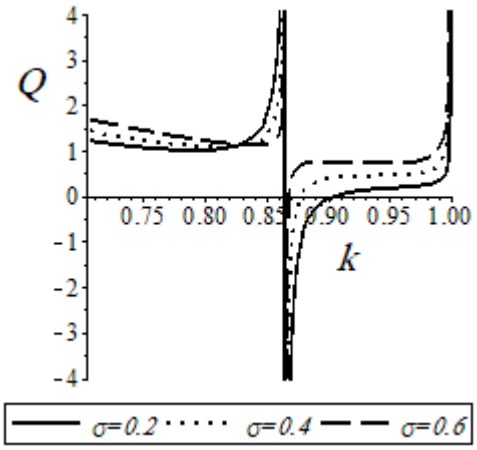


**Fig. 6.** The dimensionless nonlinear coefficient $Q$ in the NLS equation against the reduced normalized wavenumber for the forward segment of dispersion relation defined by Eq. 15 when $\sigma < 3/4$.

In the case of $\sigma > 3/4$, figure 7 illustrates the variations of $Q$ versus the wavenumber in range $\sqrt{2}/2 \leq k \leq 1$. Fig. 7b represents the zoomed curves around *k=0.865*. In this case, we observe that the variation of $Q$ versus the wavenumber for different values of $\sigma$ is similar to the forward segment, see Fig. 4 and Fig. 7b.

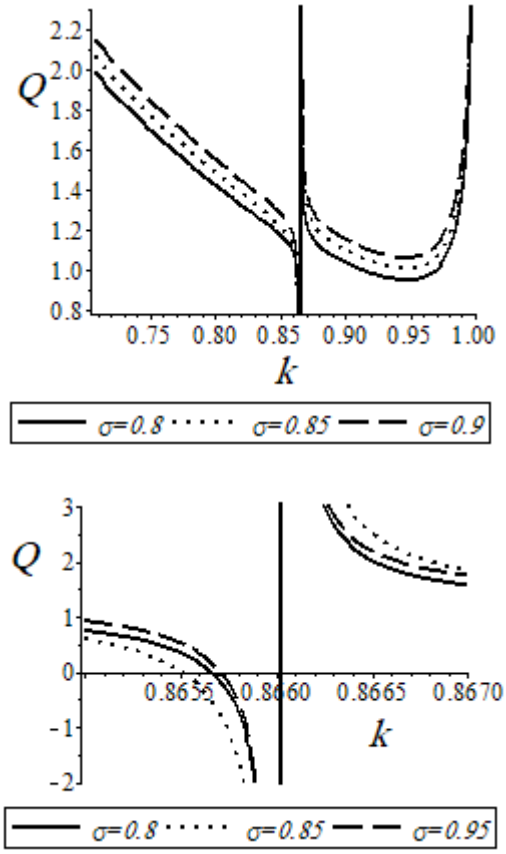


**Fig.7** a) the dimensionless nonlinear coefficient $Q$ in the NLSE against the reduced normalized wavenumber for the forward segment of dispersion relation defined by Eq. 15 when $\sigma > 3/4$, b) same plots as zoomed around *k=0.865*.

Now, let us consider the width of the space charge localized envelope excitations. The plot of *P/Q* versus the wavenumber, *k*, has been depicted in Figure 8. Focusing on the forward segment (see Fig. 8a), the width of the dark excitations will be narrower for lower wavenumbers i.e. for long wavelengths, and it increases up to infinity as $k$ increases up to $k_{ZNP}$. For $k>k_{ZNP}$, the width of the bright excitations decreases and reaches to zero at $k = k_{INP=}\sqrt{2}/3$, where the product $PQ$ changes

sign. For the wavenumbers higher than $k_{INP=}\sqrt{2}/3$ up to $k=\sqrt{2}/2$, the width of the dark excitations increases. It is seen that the characteristics of the space charge localized envelope excitations are similar for the different values of parameter $\sigma$.

Fig. 8b shows the plot of *P/Q* versus the wavenumber $k$ for $\sqrt{2}/2 \le k \le 1$ backward segment. In this case, the characteristics of the space charge localized envelope excitations vary as the parameter $\sigma$ varies (see Fig. 8b).

It should be mentioned that above results are exactly valid because $0 \le k \le 1$, consequently Landau damping will not be of importance.

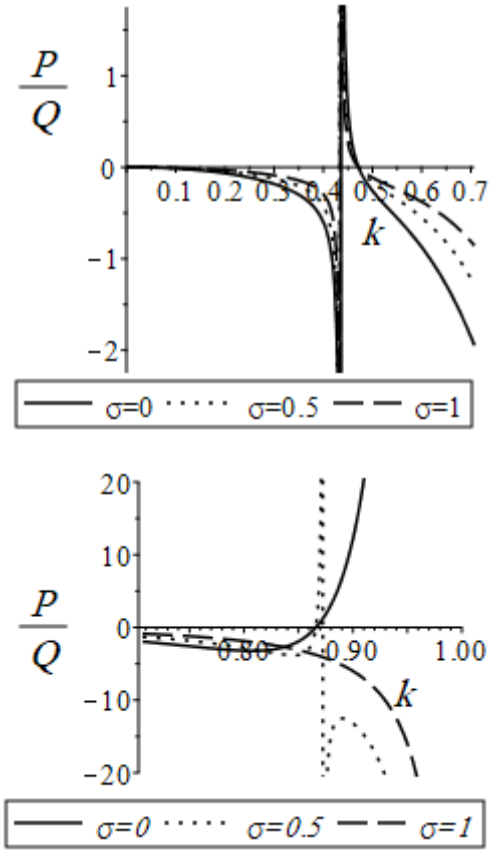


**Fig. 8** The plots of the ratio *P/Q* (whose numerical value determines the characteristics of envelope excitations) against the normalized wavenumber for different values of $\sigma$; a) for the forward segment of dispersion relation defined by Eq. 15, b) for the backward segment of dispersion relation defined by Eq. 15.

## VI. CONCLUSION

In this paper, we have considered the nonlinear propagation of space charge wave packets in a charged particle beam, by employing a water-bag distribution for the longitudinal distribution function. It has been assumed that the beam propagates through a straight, perfectly conducting cylindrical pipe with wall radius $r_w$. Linear dispersion curve of space charge waves has been obtained which consists of two forward and backward segments for the normalized wavenumbers lower and higher than $k_r=\sqrt{1/2}$, respectively. The group velocity is zero at $k_r=\sqrt{1/2}$ where the dispersion curve turns downward. The normal dispersion occurs in $0 \le k < \sqrt{-2+2\sqrt{5}}/2$ range where the magnitude of the group velocity is less than the phase one. The group and phase velocities are both positive in $0 \le k < \sqrt{2}/2$ range, i.e. forward region, while the phase (group) velocity is positive (negative) in $\sqrt{2}/2 < k < \sqrt{-2+2\sqrt{5}}/2$ range, i.e. backward region. Moreover, it was found the space charge waves illustrate anomalous dispersion for $\sqrt{-2+2\sqrt{5}}/2 < k \le 1$ region.

Considering small yet weakly nonlinear deviations from equilibrium, and adopting a multiple scale

technique, the basic set of fluid equations is reduced to nonlinear Schrödinger equation for the slowly varying linear charge density perturbation amplitude. The analysis revealed the dispersion coefficient in nonlinear Schrödinger equation (NLSE) doesn't depend on σ, and it is negative in $0 < k < 1$ range so that negative group velocity dispersion occurs. Here, $\sigma$ denotes dimensionless parameter which depends on the beam equilibrium pressure and linear charge density, electric charge of beam particle and geometric parameter $g_0$( see Eq. 3 into text). Finally, it was observed that both of stable dark and instable bright excitations associated with space charge waves can propagate not only in normal dispersion region but also in anomalous one. We hope above predictions are investigated and confirmed by appropriately designed experiments. Investigation of space charge wave packets propagation in charged particle beams in resistive-wall transport channels may be of importance which is postponed to future.

## REFENCES


[1] J. D. Lawson, The Physics of Charged-Particle Beams, 2nd ed. (Oxford University Press, New York, 1988), Chap. 6.

[2] M. Reiser, Theory and Design of Charged Particle Beams (Wiley, New York, 1994), Sec. 6.3.

[3] S. Ramo, Physical Review, Vol. 56, p.276, 1939.

[4] W. C. Hahn, Gen. Elec. Rev., 42, 258, 1939.

[5] C. Birdsall and J. Whinnery, J. of Applied Physics, Vol. 24, 3, p.314, 1953.

[6] R. O. Bangerter, Fusion Eng. Des. 32–33, 27 (1996).

[7] J. G. Wang, D. X. Wang, and M. Reiser, Physical Review Letters 71, 1993, p.1836.

[8] D. H. Dowell and P. G. O'Shea, in Proceedings of the 1997 Particle Accelerator Conference, Vancouver, BC (IEEE, New York, 1998), p. 1891.

[9] K. Bane; Y. Ding; P. Emma; J. Frisch; Z. Huang; H. Loos; F. Sannibale; K. Sonnad; G. Stupakov, J. Wu et all., in Proceedings of the 2007 Particle Accelerator Conference, Albuquerque, New Mexico (IEEE, Albuquerque, New Mexico, 2007), p. 807.

[10] H. H. Braun, R. Corsini, L. Groening, F. Zhou, A. Kabel, T. O. Raubenheimer, R. Li, and T. Limbert, Phys. Rev. ST Accel. Beams 3, 124402 (2000).

[11] G. Stupakov and S. Heifets, Phys. Rev. ST Accel. Beams 5, 054402 (2002).

[12] S. Reiche and J. B. Rosenzweig, Phys. Rev. ST Accel. Beams 6, 040702 (2003).

[13] Z. Huang, M. Borland, P. Emma, J. Wu, C. Limborg, G. Stupakov, and J. Welch, Phys. Rev. ST Accel. Beams 7, 074401 (2004).

[14] K. Tian, R. A. Kishek, I. Haber, M. Reiser, and P. G. O'Shea, PHYSICAL REVIEW SPECIAL TOPICS - ACCELERATORS AND BEAMS 13, 034201 (2010).

[15] J. C. T. Thangaraj, Ph.D thesis, University of Maryland, 2009.

[16] Y. Mo, B. Beaudoin, D. Feldman, I. Haber, R. A. Kishek, P. G. O'Shea, Proceedings of IPAC2012, New Orleans, Louisiana, USA.

[17] Ronald C. Davidson, Methods in Nonlinear Plasma Theory ACADEMIC PRESS New York and London, 1972.

[18] P. G. Drazin, R. S. Johnson, Solitons: An Introduction, Cambridge University Press, 1996.

[19] George L. Lamb, Elements of Soliton Theory, Wiley, 1980.

[20] H. Suk, J. G. Wang, and M. Reiser, Phys. Plasmas 3 (2), February 1996.

[21] Ronald C. Davidson PHYSICAL REVIEW SPECIAL TOPICS - ACCELERATORS AND BEAMS, VOLUME 7, 054402 (2004).

[22] Hans Schamel and R. Fedele, Phys. Plasmas, Vol. 7, No. 8, August 2000.

[23] C. Lan and I. D. Kaganovich, Physics of Plasmas 26, 050704 (2019).

[24] P. Sulem and C. Sulem, Nonlinear Schrödinger Equation (Springer, Berlin, 1999).

[25] J. Labelle, P. M. Kinter, A. W. Yau, and B. A. Whalen, J. Geophys. Res., vol. 91, no. A6, pp. 7113-7118, 1986.

[26] A. I. Eriksson, B. Holback, P. O. Dovner, R. Bostrom, G. Holmgren, M. Andre, L. Eliasson, and P. Kintner, Geophys. Res. Lett., vol. 21, no.17, pp. 1843-1846, 1994.

[27] I. Kourakis, A. Esfandyari-Kalejahi, and P. K. Shukla, Phys. Plasmas, vol. 13, no. 5, pp. 052117.1-052117.9, 2006.

[28] A. Esfandyari-Kalejahi, I. Kourakis, M. Mehdipoor, and P. K. Shukla, J. Phys. A: Math. Gen., vol. 39, no. 44, pp. 13817-13830, 2006.

[29] M. Salahuddin, H. Saleem, and M. Saddiq, Phys. Rev. E, vol. 66, no. 3, pp. 036407.1-036407.4, 2002.

[30] S. Sultana, and I. Kourakis, Plasma Phys. Control. Fusion, vol. 53, no. 4, pp. 045003.1-045003.18, 2011.

[31] S. Mahmood, S. Siddiqui, and N. Jehan, Phys. Plasmas, vol. 18, no. 5, pp. 052309.1-052309.7, 2011.

[32] S. Guo, and L. Mei, Phys. Plasmas, vol. 21, no. 8, pp. 82303.1-82303.9, 2014.

[33] W. S. Duan, J. Parkes, and L. Zhang, Phys. Plasmas, vol. 11, no. 8, pp. 3761-3766, 2004.

[34] S. K. El-Labany, E. K. El-Shewy, H. N. Abd El-Razek, and A. A. El-Rahman, Adv. Space Res., vol. 59, no. 8, pp. 1962-1968, 2017.

[35] Stephan I. Tzenov and Ronald C. Davidson, Proceedings of EPAC 2002, Paris, France.

[36] L.Y. Chen, N. Goldenfeld and Y. Oono, Phys. Rev. E 54, 376 (1996).

[37] K. Nozaki, Y. Oono and Y. Shiwa, Phys. Rev. E 62, 4501 (2000).

[38] K. Nozaki and Y. Oono, Phys. Rev. E 63, 046101 (2001).

[39] Y. Shiwa, Phys. Rev. E 63, 016119 (2001).

[40] R. Fedele and G. Miele, N95- 13944,1994.

[41] D. Anderson, R. Fedele, V. G. Vaccaro, M. Lisak, A. Bernston and S. Johansson, INFN/TC, 24 Nov 1998.

[42] Renato Fedele and Dusan Jovanovic AIP Conference Proceedings 740, 430 (2004).

[43] Stephan I Tzenov, New Journal of Physics 6 (2004) 19.

[44] G. Knuyt and M. Nesládek, J. Phys.: Condens. Matter 17, 227–234 (2005).

[45] M. E. Dieckmann, S. C. Chapman, A. Ynnerman, and G. Rowlands, Phys. Plasmas 7, 2681 (1999).

[46] A. Esfandyari-Kalejahi and M. Afsari-Ghazi, AIP Advances 9, 055303 (2019).

[47] V. V. Shevchenko Physics - Uspekhi 50 (3) 287 - 292 (2007).

[48] G. K. Biiagavat and D. P. Nandedkar, INT. J. ELECTRONICS, 1968, VOL. 25, NO.3 249-256.

[49] A. Sommerfeld, Annalen der Physik 44, 177 (1914).

[50] L. Brillouin, Annalen der Physik 44, 203, (1914).